From FA Smith, Applied Radiation Physics

9.3 Electrons

The most widely used modern method of accelerating electrons for clinical purposes uses a standing-wave linear accelerator operating in the S-band at 2998 MHz. This gives a wavelength of 10 cm in free space. Acceleration of electrons takes place in pulses at a repetition rate in the range 50 - 300 Hz. At a typical energy of 10 MeV, the current in the pulse is in the order of 200 mA. In this case, the power in the pulse is 10×10^6 V $\times$ 200×10^{-3} A = 2 MW. For a pulse length of 5 μS and a repetition rate of 200 Hz (5 ms between pulses), the mark-space ratio is 1000. Therefore, the mean power in the beam is 2 kW.

The electron energy distribution before the beam emerges through the final exit window depends on the type, and design, of the electron accelerator. Typical values for the energy widths – measured as Full-Width-Half-Maximum (FWHM) – are ~ 20 keV (betatron), ~ 40 keV (microtron) and ~ 50 keV (linac) [9]. After transmission through the exit window there is a downward energy shift of ~ 5% in the mean energy, as well as a broadening of approximately the same magnitude. It is this beam, with a diameter in the range 4 - 6 mm, which is transported through the bending magnets to the scattering foils.

Using the above figures for the mean power in the beam, together with a mean projected range of 5 cm for a 10 MeV electron in water, Eq.(2.5), the power density is :

$$\frac{2\times10^{3}W}{\frac{\pi\left(5\times10^{-3}\right)^{2}}{4}5\times10^{-2}m^{3}} = 2040 \text{ MW m}^{-3}$$

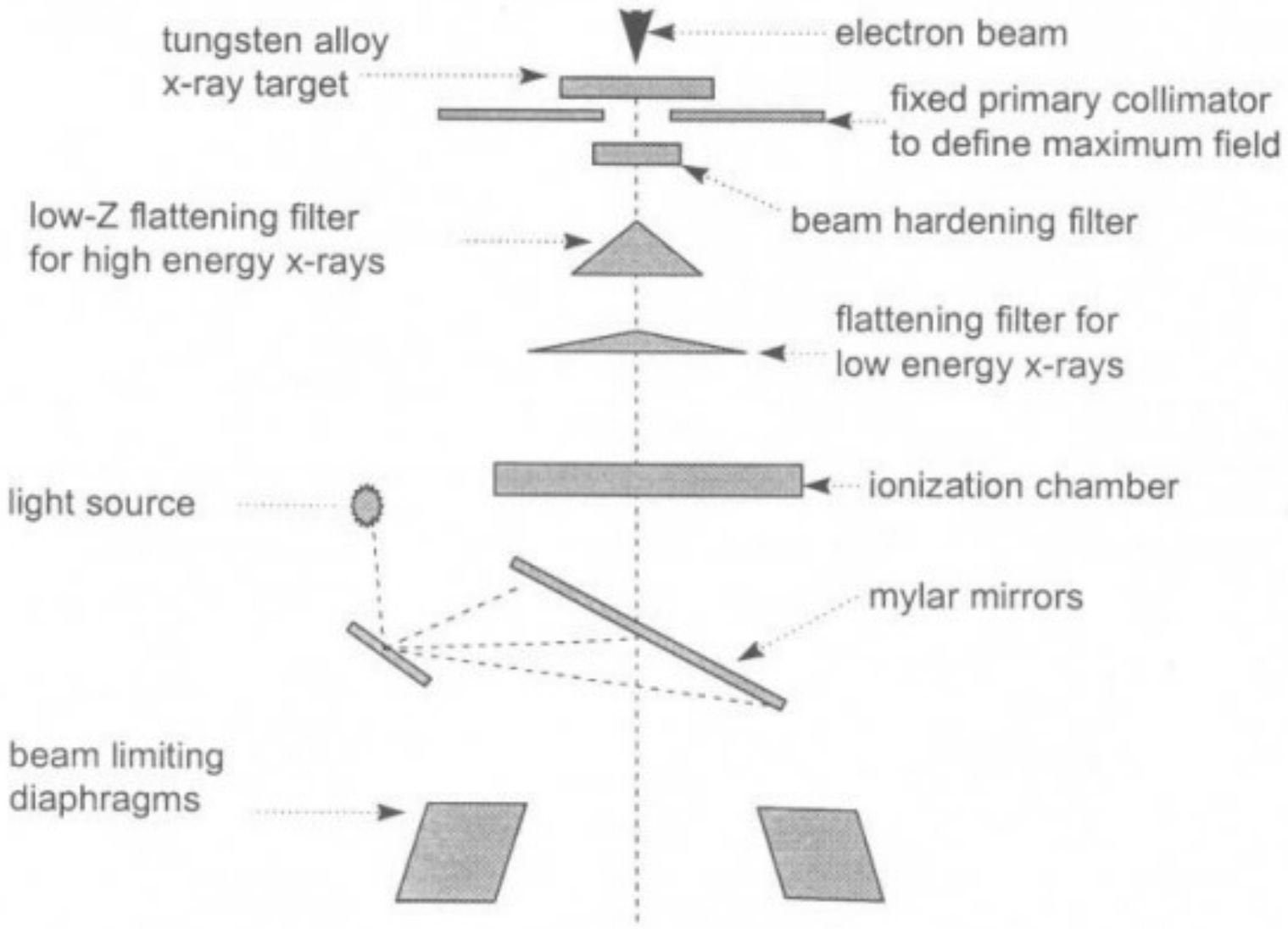

Fig.(9.24) The major components of a linac treatment head showing the arrangement of the filters for use with low-energy and high-energy x-rays.

Such a large value cannot be sustained by anything other than high melting

point materials. For therapy purposes it is therefore necessary to reduce the density either through scatter in a metallic foil or by scanning the beam over a larger area in a raster fashion. The former method of power density reduction is by far the most widely used in clinical machines.

Subsequent progress through the scatter foils, ionization chamber monitor, beam alignment foils and patient set-up mirrors will all introduce further energy degradation. A typical energy distribution at the patient/phantom surface for a nominal 10 MeV beam is shown in Fig.(9.26).

The main features of an electron therapy beam after it has emerged from the applicator and entered the phantom/patient are [10] :

- an appreciable change in energy as the electrons approach the end of their range,
- the small amount of contamination from *bremsstrahlung* and neutrons, due to electron interactions within the collimator system, and
- a much sharper fall-off in dose with depth compared with photons, Fig.(2.7).

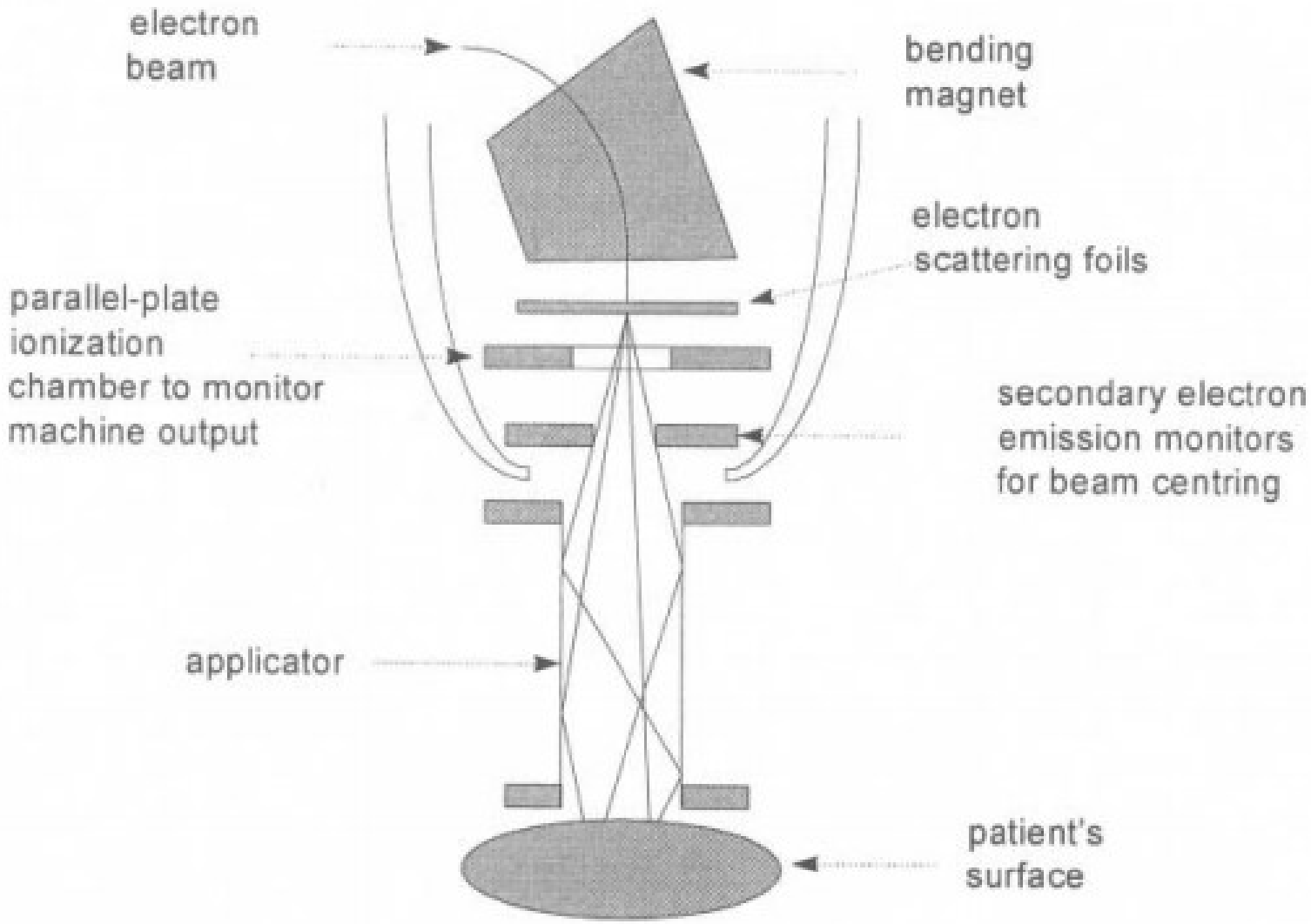

Fig.(9.25) The main features of a linac treatment head for use with electrons

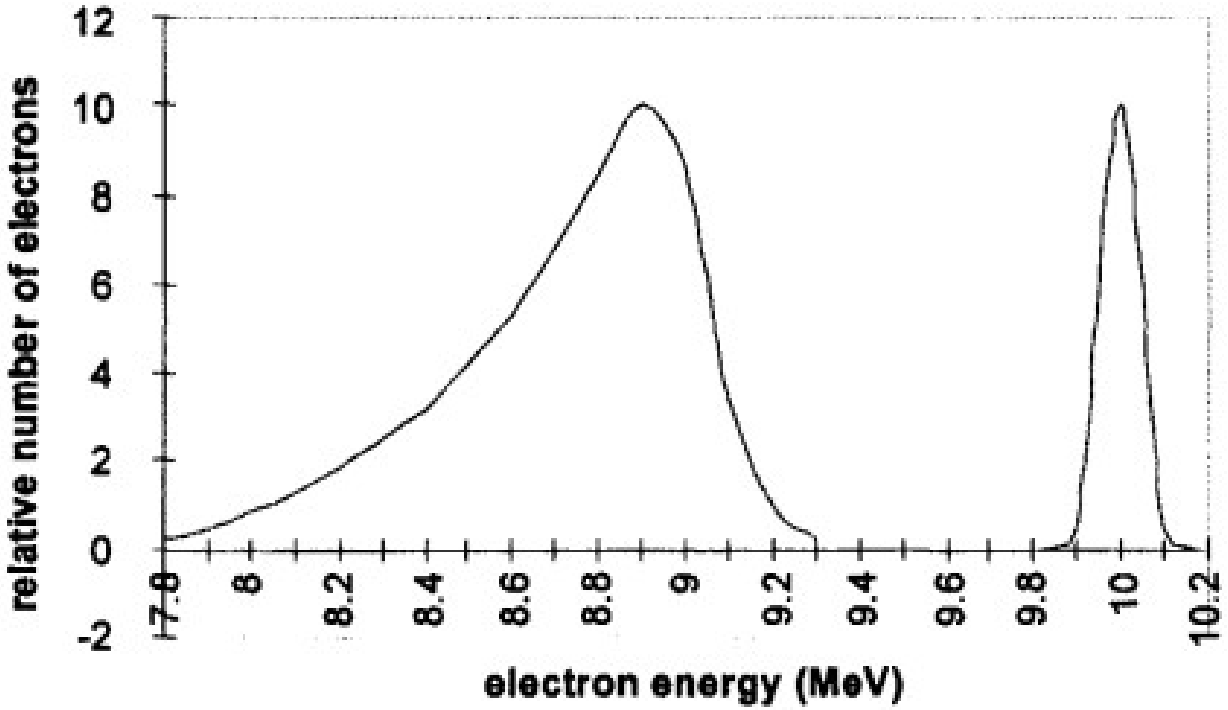

Fig.(9.26) A representation of the typical energy degradation of an electron spectrum - before emerging from the machine exit window (right) and after having passed through the filters, collimators etc. in the machine head (left). The left hand spectrum will approximate to that which irradiates the phantom/patient surface. Both energy shift and broadening vary with different arrangements of filters, applicators, SSD, etc. The most probable energies, E_p (mode), are 10.0 and 8.9 MeV. The mean energy of the degraded spectrum, E_m ~ 8.75 MeV, is lower and the maximum energy, E_{max} = 9.3 MeV, higher. The more the energy spectrum becomes degraded the larger the difference between the mean and mode energies due to the increasing asymmetry of the distribution [10]. For the purpose of illustration, the integrated area of the right hand spectrum has been reduced.

9.3.1 *Determination of electron energy at depth in the phantom*

In view of the differences between mean, modal and maximum energies of the electron spectrum and their intimate relationship with dosimetry, it is essential to be able to relate the selected machine energy with the energy at a specified depth in the phantom.

Harder [11] has shown that a linear dependence of the most probable energy on depth exists for all but the largest depths :

$$E_{p,z} = E_{p,0}\left(1 - \frac{z}{R_p}\right) \tag{9.8}$$

where the additional subscripts, *z* and *0*, refer to depth and surface respectively. R_p is the practical range of the electron beam, Fig.(2.7). This relation extends also to the mean energies $E_{m,z}$ and $E_{m,0}$ with less, but acceptable, accuracy.

Under the assumption that collision stopping power is relatively constant with energy, and radiative stopping power is directly proportional to mean energy, Andreo and Brahme [12] derived an exponential relation between mean energy and depth :

$$E_{m,z} = E_{m,0} \frac{S_{tot}\ exp\left(-\frac{zS_{rad}}{E_{m,0}}\right) - S_{coll}}{S_{rad}}$$

The stopping powers S_{tot}, S_{coll} and S_{rad} are quoted at the mean energy $E_{m,0}$ in the phantom material. When the exponential term is expanded, we get :

$$E_{m,z} = E_{m,0} - z\ S_{tot}\left[1 - \frac{S_{rad}(E_{m,0})\ z}{2\ E_{m,0}}\right] \qquad (9.9)$$

Deviation from the linear expression in Eq.(9.8) is only significant near the end of the electron range.

From the point of view of dosimetry, the specification of beam energy is most sensibly based on the most probable energy at the phantom surface, $E_{p,0}$. This then permits the comparison of one beam with another to be made solely on the basis of the phantom geometry and material, SSD, field size, etc. and not on any of the machine parameters, such as filters or other components of the beam handling system. When this is done, the settings on the accelerator can then be calibrated against this most probable energy.

There are three principal methods that are available for a determination of the primary electron beam energy. They are, however, not generally available in a medical physics department and are also not generally the most appropriate for energies below 20 MeV.

- Magnetic spectrometry: This uses the relation between magnetic field strength B, radius of curvature r and particle momentum p, and hence E, when the B and r are known. If e is the electronic charge and E_0 the electron rest energy, (0.511 MeV) :

$$p = Ber \qquad \text{and} \qquad p = \frac{1}{c}\sqrt{E(E+2E_0)}$$

- Nuclear reactions: This relies on the production of measurable radioactivity of a foil which is initiated by an incident electron or photon whose energy is above the reaction threshold. The foil activity is measured as the energy is reduced from above the threshold until no activity is measurable. Reactions of the type (e,e'n) and (γ,n) are used (see Chapter 8). Although there are many elements which have thresholds between 10 and 30 MeV, there are very few – e.g ^{109}Ag with a threshold of 9.3 MeV [13] – below this range.
- Cerenkov radiation: This method rests on the emission of optical radiation when

a charged particle passes through a dielectric medium with a velocity greater than the phase velocity of light in that medium. For a medium of refractive index n and a particle of velocity $v = \beta c$, the condition $\beta n > 1$ gives rise to the emission of light within a cone of semi-angle φ such that $\sin\varphi = 1/\beta n$. If n is known, the point at which light ceases to be emitted within the cone gives the value of β and hence the particle energy. This method is largely restricted to energies greater than 30 MeV where the other methods become less convenient.

The most useful practical method of energy determination, however, is to use empirical range-energy relations. These have been developed using the results of Monte-Carlo calculations and an analysis of experimental depth-ionization or depth-absorbed dose data, Figs.(2.6) and (2.7).

Using a calibrated β-spectrometer, Markus [14] determined a relation valid between 3 and 15 MeV in low atomic number materials. The practical range, R_p, is related to the most probable energy, $E_{p,0}$, at the surface of a phantom of density ρ by:

$$\rho R_p \frac{Z}{A} = 0.285 E_{p,0} - 0.137 \qquad (9.10)$$

where Z/A is the ratio of the mean atomic number to atomic mass (Z/A = 0.555 for water). Eq.(9.10) has been found to agree with experimental data to within 0.43% in the range 3 - 15 MeV and 1.9% for 3 - 30 MeV [15].

At higher energies, where radiative energy losses become increasingly important, the relation becomes non-linear. In the range 1 - 50 MeV the expression :

$$E_{p,0} = 0.22 + 1.98 R_p + 0.0025 R_p^{\,2} \qquad (9.11)$$

gives agreement to within ~2%.

An equally important set of relations comes from the results of Monte Carlo calculations. These suggest that the mean beam energy, $E_{m,0}$, is related to the depth at which the absorbed dose falls to 50% of its peak value, R_{50}, Fig.(2.7). The ease with which R_{50} can be measured, and the importance of $E_{m,0}$ in defining the correct stopping power data for dosimetry calculations, prompted the recommendation :

$$E_{m,0} = 2.4R_{50} \qquad (9.12)$$

For Eq.(9.12) to be valid, R_{50} must be measured using a constant source chamber distance rather than a constant SSD which is usually the case for a conventional depth dose determination. A recent review of these relationships has been given by

Fernandez-Varea et.al. [16]. A summary of the values in water is taken from [9].

However, the more recent IPEMB electron dosimetry code of practice [17] specifies a constant SSD of 100 cm and distinguishes between :

- $R_{50,D}$ = the depth at which the dose is 50% of the maximum, and
- $R_{50,I}$ = the depth at which the ionization is 50% of the maximum.

This distinction is necessary in absolute dosimetry because an ionization chamber measures only the number of ionizations per unit mass of chamber gas without any consideration of the resulting secondary electron energy spectrum. However, the absorbed dose depends on the mass collision stopping powers of the secondary electrons averaged over the electron fluence. Account should therefore be taken of the increased secondary electron ranges at high primary electron energies. If this is not done, the dose averaged over a small volume at a given point will underestimate the primary electron energy. Furthermore, expressions such as Eq.(9.12) assume a mono-energetic, mono-directional and uncontaminated primary beam. None of these restrictions apply in practice.

The corrected expressions now recommended [17] are therefore :

$$E_{m,0} = 0.818 + 1.935R_{50,I} + 0.040(R_{50,I})^2$$
$$E_{m,0} = 0.656 + 2.059R_{50,D} + 0.022(R_{50,D})^2 \qquad (9.13)$$

where E is in MeV and R is in cm. A difference between $R_{50,I}$ and $R_{50,D}$ in water at an SSD of 100 cm becomes apparent at an electron energy of ~14 MeV above which $R_{50,D}$ is larger by ~2%. For the same reasons, Eq.(9.8) is no longer recommended for accurate work.

9.3.2 Bremsstrahlung contamination of electron beams

There are two sources of photon contamination in an electron beam and each contributes rather differently to the overall depth dose distribution. These are :

- Treatment-head photons. The generation of these photons begins as soon as the energetic electrons leave the UHV conditions of the accelerator tube. This is because of the need for high-strength, high-thermal-conductivity materials to withstand the large energy-density radiation in the head of the accelerator. The exit window of the waveguide, scattering foils, ionization chamber and collimator walls will all tend to have high atomic numbers and high densities and will therefore provide ideal targets for unwanted X-ray production.
- Phantom-generated photons. This smaller contribution can come from anywhere within the phantom. They can be generated at any point between the surface and the depth of the practical electron range, R_p, and with all energies up to the allowed maximum.

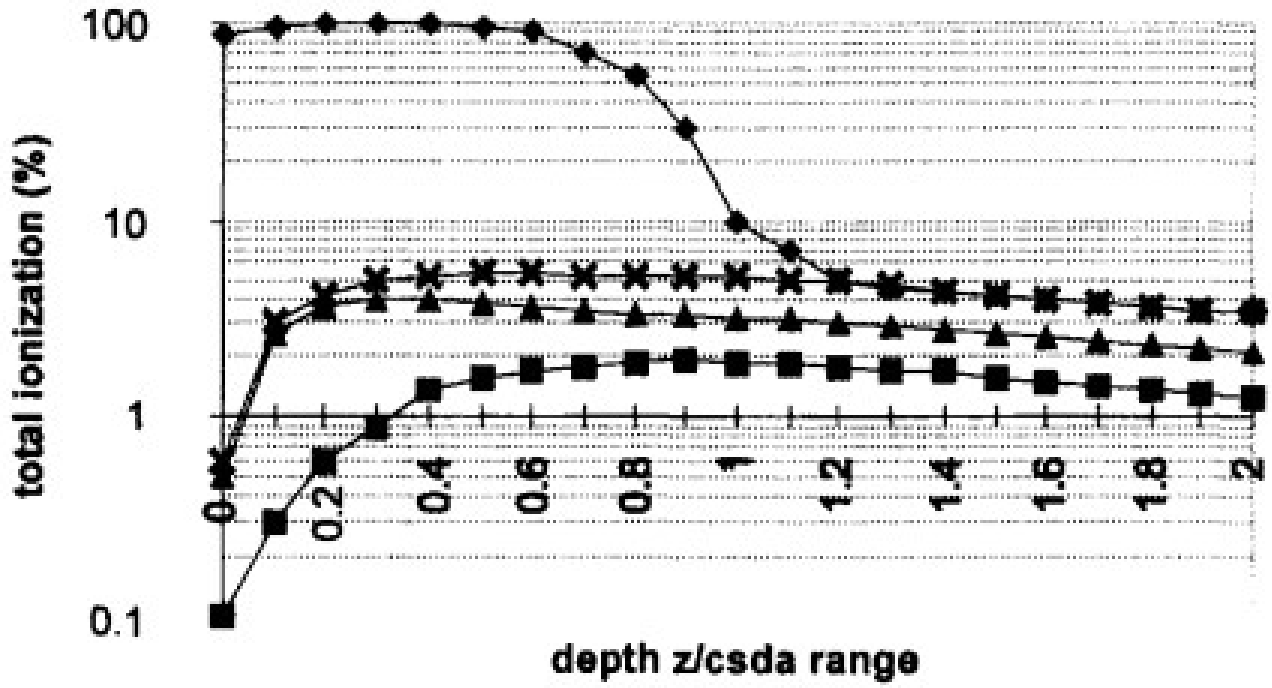

Fig.(9.27) Total percentage ionization versus z/r_0 calculated for 20 MeV electrons in water [20]. z is the real depth in the phantom and r_0 = 9.18 cm is the csda range of a 20 MeV electron in water. ◆ ionization due to primary electrons ; ■ ionization due to phantom-generated bremsstrahlung ; ▲ ionization due to accelerator-generated bremsstrahlung ; ✖ total bremsstrahlung ionization.

Independent experimental determinations of these contributions are difficult. The major component – from the accelerator head – can be found by magnetically deflecting the primary electron beam away from the phantom so that it is only the photons that contribute to the depth dose. The alternative is to extrapolate the depth dose data from beyond the practical range of the primary electrons using a combination of inverse square law and exponential attenuation. The latter method has been used, [18] [19], to produce an algorithm to describe the major contribution from the treatment head. Monte Carlo simulations [20] are, of course, capable of distinguishing between each of the two contributions.

Fig.(9.27) shows the total ionization measured in a water phantom irradiated by 20 MeV electrons [20]. The contributions due to primary electrons, and to photons generated in the treatment head and within the phantom itself, are shown as a function of depth normalized to the csda range of the incident electrons. Note that the maxima in each of these components occurs at $z/r_0 = 0.3$ and 0.9 respectively and show a photon component of ~ 4.5% at the total dose maximum.

At the lower treatment energies, 6 MeV and 8 MeV, *bremsstrahlung* contamination tends to be ~1%.

9.4 Heavy Particles

Radiobiological arguments for using heavy particles for therapy rest on the empirical evidence which shows the dependence of two radiobiology parameters – Relative Biological Effectiveness (RBE) and Oxygen Enhancement Ratio (OER) – on the physical parameter Linear Energy Transfer (LET).

- LET is defined as the loss of energy ΔT by a charged particle as the result of electronic collisions which take place along a track length Δx. It is therefore equal to the collision stopping power, with the proviso that account must be taken of the electron cut-off energies (section 2.5.2). LET_{∞} is the total collision stopping power.
- RBE of a certain radiation is defined as the ratio :

  $$\frac{\text{dose of a reference radiation to produce a certain biological end-point}}{\text{dose of the certain radiation to give the same end-point}}$$

  The reference radiation is generally 250 kV X-rays. An irradiation with X-rays therefore has an RBE = 1, by definition.
- OER is defined as the ratio :

  $$\frac{\text{dose required to give a certain effect in the absence of oxygen}}{\text{dose required to give the same effect in the presence of oxygen}}$$

Fig.(9.28) shows that X-rays generally have a high OER (~3) and therefore require 3 times more dose to kill the hypoxic tumour cells than the surrounding well-oxygenated normal cells. As the LET increases towards 100 eV nm^{-1}, the rise in RBE and fall in OER indicate the real advantages in using high LET radiation for therapy.

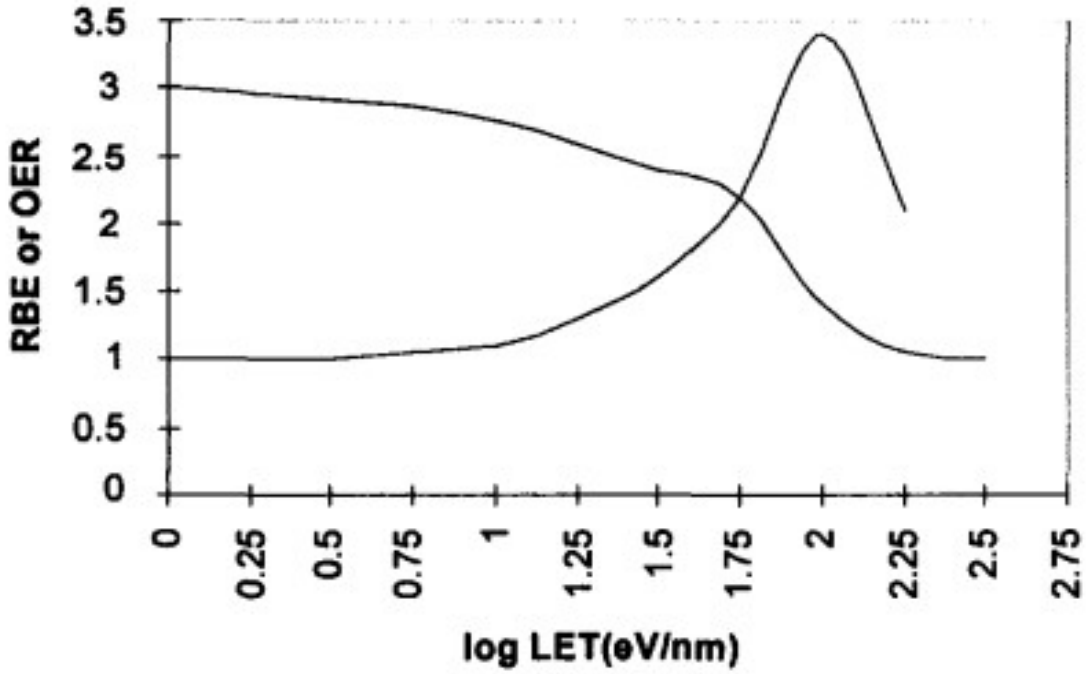

Fig.(9.28) Representative empirical relations showing the fall in OER with LET and the increase in RBE from unity at low LET to a maximum of ~ 3.5 at 100 eV nm^{-1}. These are based on the results of many radiobiological studies of mammalian cells using a number of different biological end-points.

In addition to the radiobiological advantages of using charged heavy particles for therapy, there are also good physical reasons for doing so. These rest on the high stopping powers and short ranges, even in low Z and unit density materials. Stopping power of a heavy charged particle rises to a maximum as the particle approaches the end of its range, Fig.(2.25). A beam of charged particles therefore produces a dose maximum which is referred to as the Bragg Peak. This occurs for protons in water when the mean proton energy has fallen to ~ 100 keV at which point the mean stopping power is ~ 100 keV μm^{-1}. Although the ultimate secondary particle produced from heavy particle interactions is the electron in all cases, intermediate products arise in external beams of neutrons, negative pions and heavy ions to give particular energy deposition characteristics.

In any radiation field in which there is more than one component (*e.g.* electrons and X-rays, neutrons and γ-rays, protons and electrons...), the isodose contours

Table (9.5) Secondary particles produced from heavy primary particles.

primary particle	intermediate particles	ultimate particle
proton	-	electron
neutron	protons, α-particles, γ-rays	electron
negative pion	protons, deuterons, tritons, He ions, etc	electron
heavy ions	fragmentation products	electron

Fig.(9.29) Depth dose (MeV cm^2 g^{-1}) for 200 MeV monoenergetic protons in water [21] versus z/r_0. (Note the suppressed zero on the abscissa axis and the unconventional dose units).
The dose maximum, D_m, occurs at depth z_m. The dose at the csda range ($z/r_0 = 1$) is D_{rg}. The width of the Bragg peak at 50% of D_m is w_{50}, and the distal depth (behind the peak) at which the dose falls to 50% is z_{50}.
For 200 MeV protons in water the above parameters are : r_0 = 27 cm : D_m = 24 MeV cm^2 g^{-1} : D_{rg} = 18 MeV cm^2 g^{-1} : $z_m = 0.99 \times 27 = 26.7$ cm : $w_{50} = (1.006 - 0.927) \times 27 = 1.86$ cm : $z_{50} = 1.006 \times 27 = 27.2$ cm. Data taken from [22].

are often different to the iso-effect contours. Iso-effect contours refer to a particular biological end-point such as cell death, chromosome aberration, etc. This is because of the different micro-dosimetry associated with different charged secondary particles, Fig.(2.17). Even the same particle (*e.g.* an electron), will have different energy spectra when produced from different initial particles. This is particularly the case in hadron therapy (heavy charged particles) where heavy secondaries (*e.g.* protons, He ions…) as well as electrons contribute to the overall dose.